We are IntechOpen,
the world's leading publisher of
Open Access books
Built by scientists, for scientists

4,800
Open access books available

122,000
International authors and editors

135M
Downloads

Our authors are among the

154
Countries delivered to

TOP 1%
most cited scientists

12.2%
Contributors from top 500 universities

CLARIVATE ANALYTICS
BOOK CITATION INDEX
INDEXED

WEB OF SCIENCE™

Selection of our books indexed in the Book Citation Index
in Web of Science™ Core Collection (BKCI)

Interested in publishing with us?
Contact book.department@intechopen.com

Numbers displayed above are based on latest data collected.
For more information visit www.intechopen.com

Recent Advances in Converters and Control Systems for Grid-Connected Small Wind Turbines

Mohamed Aner, Edwin Nowicki and David Wood

Additional information is available at the end of the chapter

http://dx.doi.org/10.5772/51148

1. Introduction

In response to the introduction of feed-in tariffs around the world, an increasing number of small wind turbines are being grid connected [1]. Variable speed wind turbines, though initially more costly, have several advantages over fixed speed systems: (i) average power production is typically 10% higher since the turbine operates more frequently near its ideal tip-speed-ratio, (ii) the turbine and mechanical transmission operate with reduced stresses, (iii) turbine and generator torque pulsations are reduced, and (iv) noise is reduced [2-4]. Variable speed operation in general has only become possible over the last twenty years or so because of major developments in power electronics and associated cost reductions [5]. This reference indicates that power electronic devices are reducing in cost at about 1-5% per year. This chapter will discuss the impact of these developments on small turbine design and operation along with some important aerodynamics issues related to turbine starting.

The blades of most small horizontal-axis wind turbines (HAWTs) have no pitch adjustment. This reduces their cost but makes starting and low wind speed performance a major challenge. In order to extract the maximum possible energy available from the wind, power extraction should begin at the smallest possible wind speed in the shortest possible time. Few researchers have examined wind turbine starting. Ebert and Wood [6] and Mayer et al. [7] measured starting sequences from separate 5 kW HAWTs. Kjellin and Bernhoff [8] developed a scheme for starting a small vertical axis wind turbine (VAWT) using auxiliary generator windings that are not used for power production. Hill et al. [9] discuss the aerodynamic starting of Darrieus VAWTs which have problems similar to, or worse than, those for HAWTs. The remainder of this chapter considers only HAWTs with fixed-pitch blades configured with an AC generator and power converter that delivers fixed frequency electrical power while allowing the turbine to operate at variable rotational speeds.

The lack of pitch adjustment in small wind turbines (considered here to have a rated power output of 50 kW or less) means the blades experience high angles of attack during starting and, hence, low lift to drag ratios. Moreover, most small wind turbines employ permanent magnet synchronous generators (PMSGs) whose cogging torque[1] can have a significant impact on starting. Wood [13] showed that the cogging torque must be less than 1% of the rated torque to be unimportant. Partly because of high cogging torque, the blades of the 500 W HAWT studied by Wright & Wood [11] did not start for a wind speed below 5 m/s approximately, whereas the conventionally-measured cut-in wind speed was 3.5 m/s. The difference was due to the blades' ability to keep rotating as the wind speed decreased below 5 m/s. In other words, the "stopping" wind speed of a HAWT is significantly lower than the aerodynamic "starting" speed and the cut-in speed is some average of the two. It is also noted that 5 m/s is a typical average wind speed for locations where a small turbine is likely to be employed. Wood [10] described the multi-dimensional optimization of blade design including the minimization of starting time. Subsequent tests on 2.5 m long 5 kW blades designed for good aerodynamic starting are described below. From rest, they take about 13 s to reach the power-extracting angular velocity at a wind speed of 10 m/s and about 40 s at 3 m/s. These times can result in a significant loss of output energy compared to operation with much faster starting times.

As modern small wind turbine systems evolve, several issues are emerging that may be effectively and economically dealt with by the use of modern power electronics. While many small turbines operate with variable rotor speed, it is uncommon for their power electronics to allow power flow to and from the grid. In fact, many small turbines are sold with only a diode rectifier or battery charger. The diode rectifier configuration (either a four diode full-bridge for a single-phase generator or a six diode full-bridge for a three-phase generator) is often used because of its simplicity, reliability and economy. A battery charger may be added, in the form of a single-transistor based buck converter or boost converter. Both the diode rectifier and the battery charger allow power flow in one direction only (from generator to a DC capacitor or battery), which to date has been satisfactory, but as suggested below, bi-directional converters may be used in the near future to extract more energy from small wind turbines.

With the conventional diode rectifier based system, small wind turbines normally require a third party inverter for grid connection. This inverter often has to provide the maximum power point tracking (MPPT) for optimal power extraction. In turn, many such inverters are based on photovoltaic inverters for which the "perturb and observe" (P & O) strategy for MPPT is effective [12]. P & O does not work well for wind turbines because of the (usually) rapidly changing wind speed and most sophisticated small turbines with integral inverters base their MPPT on some form of look table for maximum power as a function of generator frequency. Thus the basic operation of small wind turbine inverters needs to be fundamentally different from those used for photovoltaics.

---

1 By "cogging torque" we mean the maximum value of the phase-dependent cogging torque. The value is independent of the direction of rotation.

Another particular issue is the need to have high rectifier efficiency and high inverter efficiency over a very wide range of power levels. In principle, this is also a requirement for large turbines, but the lower average wind speeds seen by small turbines makes the low power performance especially important. Many commercial small inverters now have efficiencies of over 95% at rated power but drop off alarmingly at lower power levels due to losses in filter, transformer, and controller components (such losses are much more significant in small power converters than in high power converters). The development of modern semiconductor switching devices and advances in high frequency switching control continue to be crucial to the extension of high efficiency operation in low wind speed (i.e. low power) regimes.

Another power electronics issue of rapidly increasing importance is that of AC power quality. At very small power levels (below 500W), where economy is a driving market requirement, the inverter operates with a simple controller that produces a modified square-wave AC output voltage (i.e. a square wave modified by the addition a zero voltage step between negative and positive voltage levels). Such inverter operation is reliable, with low switching losses (since the transistors are switched at the power frequency of 50Hz or 60Hz) and without any need for filter components. The total harmonic distortion (THD) is a measure of deviation from a sinusoidal waveform; for a typical modified square wave the THD is about 30%. However with increasing use of renewable energy sources, it is very possible that in the near future national electronic equipment standards will require manufacturers of small inverters to produce AC voltage (or AC current in the case of grid-connection) having a THD on the order of 5% or even lower. Since about 1990, inverters with a power output above 2kW have increasingly been manufactured with pulse width modulation (PWM) that rapidly (in the range of 1kHz to 10kHz) switches transistors such that the transistor bridge output can be filtered with low cost inductor and/or capacitor components to produce AC output current with low THD for grid connection. It is expected that PWM will become more commonly used even at the very low power levels of a few hundred Watts.

One problem with PWM operation is the issue of increased cost and reduced reliability resulting from the use of the required filter components (without filtering the THD would be well above 100%). A trend that is in its infancy for high power inverters may one day be applied to lower power inverters is the multilevel inverter, which produces a stair-stepped approximation of a sinusoidal voltage or current and requires little filtering (or even no filter if PWM is not used at all and there are a sufficient number of levels). A significant disadvantage of the multilevel inverter is an increase in the number semiconductor power transistors, and hence decreased reliability and increased cost. However with rapidly evolving power semiconductor switching technology, multilevel inverters may one day become economical even at lower power levels.

In this chapter, the focus is on the issue of bi-directional power flow in the power converter of a small wind turbine system. Bi-directionality of power flow is an example of what is now available (and quickly becoming more economical) using modern power electronics. This chapter presents one such system and explores its use in motor-starting a small wind turbine to reduce the starting time. The ideal case of turbine starting after the wind speed

makes a step change from zero to a constant value, *U*, within the turbine operating range is considered, and any issues regarding the measuring of *U* is ignored. It is also assumed that power extraction takes over instantaneously from starting at a nominated rotor angular velocity. The justification is that if motor-starting for this case results in an energy gain, it is worth pursuing. If it does not, then it is to be discarded. We show that motor-starting is worth pursuing

The following sections present the electrical system in which motoring and generating modes are controlled by field oriented control (FOC) through a bi-directional very sparse matrix converter (VSMC) which is connected in a backward configuration (i.e. the "rectifier" portion of the VSMC is connected to the grid and the "inverter" portion is connected to the generator). This allows a sufficient DC-link voltage for grid connection at any wind speed while the system is in the generating mode, and also permits straightforward grid synchronization where power is regulated by current control, depending on grid voltage to avoid voltage flicker. In addition, by using a small filter, sinusoidal current can be injected into the grid at unity power factor (or slightly leading or lagging power factor as desired) to improve power quality [13]. An alternative to the VSMC is the well known back-to-back converter (where the rectifier is implemented with a conventional inverter structure). However, the back-to-back converter requires some form of DC-link storage such as a capacitor, which is not the case for the a VSMC.

One particular recent power electronics development of interest for matrix converters is the emergence of the Reverse Blocking IGBT (RB-IGBT) which has become commercially available and tested for matrix converter implementations. It has been shown [14] that the conduction losses, switching losses, and conduction voltage of RB-IGBTs are lower than the current generation IGBTs which should lead to higher converter efficiencies. Another recent power electronics development is the commercialization of the Bi-directional Reverse Blocking IGBT (BRB-IGBT) for use in high power converters which may one day be used in lower power converters. A prime candidate for such switching technology is the matrix converter and its derivatives. Matrix converters (having the ability for extremely flexible bi-directional control of power in three-phase systems) in their conventional (non-sparse) form have long been criticized because of the high cost and high power losses associated with a high transistor and diode count (e.g. 18 transistors and 18 diodes in one particular form). The use of bi-directional reverse blocking devices would remove the need for external reverse voltage blocking diodes, and reduce the control requirements of a full matrix converter (only nine devices to be controlled), as well as reduce power losses in the converter. Thus, BRB-IGBT devices may lead to economical matrix-based or other converter configurations with lower power losses and simplified gate drive requirements [15, 16]. The study discussed below, uses an established implementation of bi-directional power flow in a power switch, namely, a conventional IGBT transistor within a four-diode bridge as shown in Fig.1 (the diodes provide both reverse voltage blocking capability and bi-directional power flow control). This configuration has the advantage of a simplified switch drive circuit (only one IGBT needs to be controlled regardless of power flow) but the disadvantage of increased conduction losses in two conducting diodes. An alternative bi-directional power switch configuration consists

of two anti-parallel IGBT (or other transistor) devices, each with a reverse blocking diode, which would reduce the losses (only one conducting diode) but require a more complicated transistor driver (two transistors need to be controlled for each bi-directional switch). Figure 2 shows the configuration of VSMC built with BRB-IGBT switching devices.

Section 3 describes a 5 kW wind turbine and its starting performance. An expression for the energy gain (i.e. harvested and delivered to the grid) is derived using the proposed motoring approach verses aerodynamic starting. Section 4 presents the model and operation of the PMSG and the VSMC in the backward configuration, including a space vector modulation approach. Then in Section 5, the simulation results for a 5.6 kW wind turbine are presented, including a plot of energy gain as a function of wind speed which compares well with the analytical result presented in Section 4. Conclusions are presented in Section 6.

2. Small wind turbine system configuration with VSMC

Figure 1 illustrates the proposed HAWT, including a PMSG connected to the grid through a backward very sparse matrix converter (where the rectifier side is connected to the grid and the inverter side is connected to the generator). Fig. 1 also shows the maximum power point tracking (MPPT) controller. The current flowing to or from the generator is controlled by field oriented control (FOC). The system operates as follows. Once blade rotation is detected, the generator is operated as a motor with the rated electromagnetic torque in the same direction as the aerodynamic torque until it reaches the nominated speed for power extraction where the MPPT unit takes control to keep the turbine operating at the optimal tip speed ratio (λ_{opt}). The reference torque is converted to a reference generator current through the FOC unit and compared to the actual current to generate the appropriate generator voltage. Then the reference voltage based on space vector modulation forms the switching signals to the VSMC.

The turbine power output, P_m, is expressed in conventional form as:

$$P_m = 0.5 \rho A C_P U^3 \tag{1}$$

where ρ is the air density, A is the rotor swept area, U is the wind speed and C_P is the turbine power coefficient which is related to the torque coefficient, C_T, by

$$C_P = C_T \lambda \tag{2}$$

where λ is the tip speed ratio. C_T is approximated by [17]:

$$C_T = a_6 \lambda^6 + a_5 \lambda^5 + a_4 \lambda^4 + a_3 \lambda^3 + a_2 \lambda^2 + a_1 \lambda + a_0 \tag{3}$$

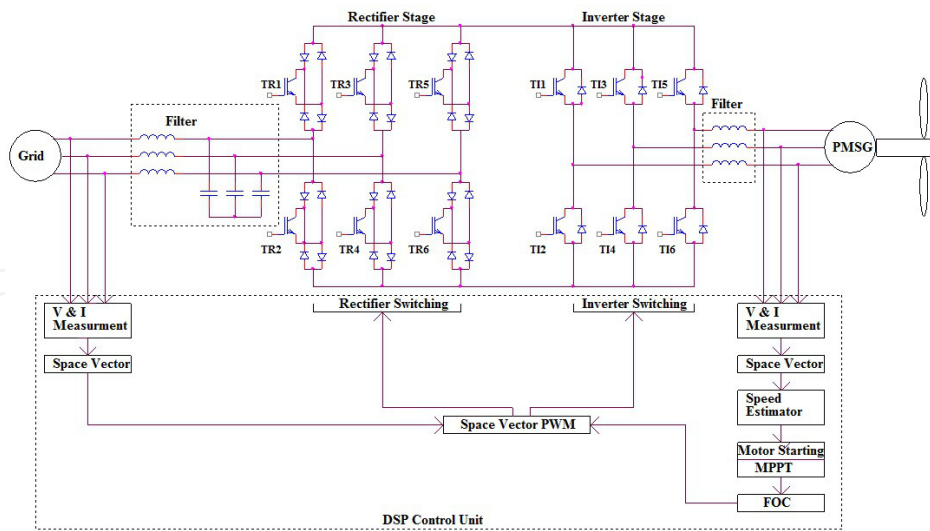where a_6 to a_0 are turbine coefficients defined in the Appendix.

Figure 1. Proposed grid connected HAWT system using backward VSMC.

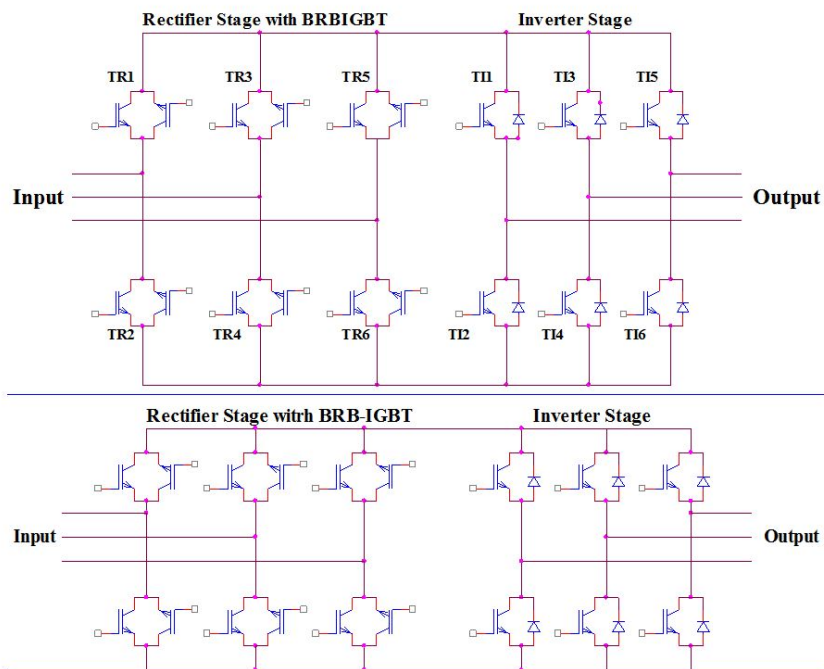**Figure 2.** Alternative implementation of the backward VSMC using BRB-IGBT devices.

Figure 3 shows the variation of C_T form Equation (3) versus λ for a 5.6 kW wind turbine whose other parameters, taken to be typical of a wind turbines of that output, are given in the Appendix. Also shown is the measured starting performance of a 5.0 kW turbine whose blades were designed for rapid starting using the methods described by Wood [10]. In Figure 3, a 5th order curve is fitted to the measured starting data, but more important, a linear approximation is also determined and used for simulation of motoring. It is important to

note that the C_T from Equation (3) applies only when power is being extracted. The starting turbine does not extract power so the wind speed does not decrease through the rotor, and the blade aerodynamics is fundamentally different. The starting line and the curve from Equation (3), intersect close to $\lambda \approx 7$ which is approximately the optimum tip speed ratio. This allows the controller to employ the linear plot for motoring and then switch to the steady aerodynamic curve from Equation (3) for power generation.

3. The aerodynamic of starting and energy gain by motoring

Figure 4 shows starting data of a 5.0 kW wind turbine, in terms of wind speed and tip speed ratio as a function of time. The 5 m diameter, two-bladed 5.0 kW turbine had fixed-pitch blades designed for good aerodynamic starting (without motoring). Even at a high wind speed of around 10 m/s the blades take about 13 s to reach the minimum angular velocity for power extraction.

Starting can be analyzed using standard blade element theory with no axial or azimuthal in-duction, Wood [10]. With all lengths normalized by the blade tip radius, R, and all velocities normalized by U, the aerodynamic torque, Ta, acting on the starting rotor, is given by
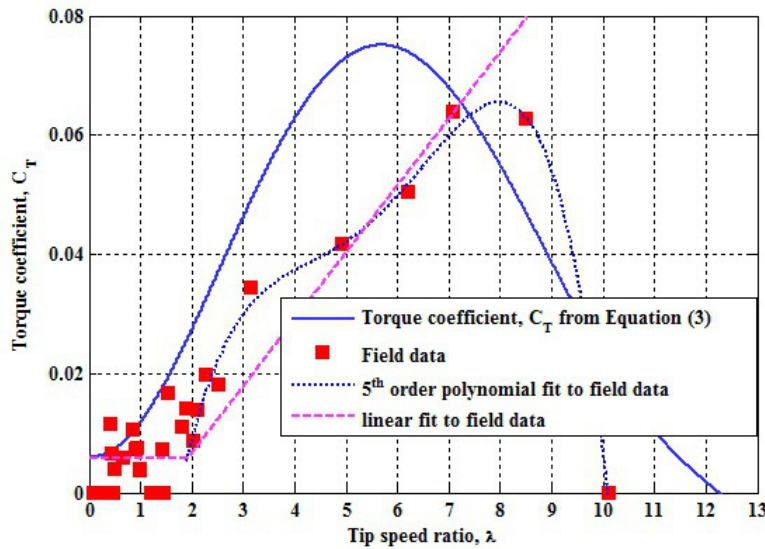

Figure 3. Measured starting torque for a 5 kW wind turbine and assumed power-extracting torque for a 5.6 kW wind turbine.

$$T_a = N\rho U^2 R^3 \int_{r_h}^1 (1 + \lambda^2 r^2)^{1/2} r \sin\theta_p (\cos\theta_p - \lambda r \sin\theta_p) dr \qquad (4)$$

where N is the number of blades, c is the blade chord which depends on radius r, and θ_p is the pitch. The integration is from the normalized hub radius, r_h, to the tip. Equation (5) is derived in [10] where the assumptions behind it are justified in detail. In particular, it is assumed that the angular acceleration is small enough to allow a quasi-steady analysis and the lift and drag on any airfoil are given by the "flat plate" equations:

$$C_l = 2\sin\alpha\cos\alpha \quad \text{and} \quad C_d = 2\sin^2\alpha \tag{5}$$

which are valid for angles of attack, $\alpha > 30°$ approximately. As no power is extracted the rotor torque T_a acts only to accelerate the blades. Thus:

$$d\Omega/dt = (T_a - T_r)/J \quad \text{or} \quad d\lambda/dt = (T_a - T_r)/(JU) \tag{6}$$

where J is the total rotational inertia and T_r is the resistive torque due to cogging torque or resistance in the gearbox which may or may not depend on Ω. For the start shown in Figure 3 and 4, T_r was negligible and the torque was inferred from Equation (6) and the turbine inertia. It is shown in [10] that for wind turbines of any size, $J \approx NJ_b$ where J_b is the inertia of each blade. In words, the turbine inertia is dominated by the blades as can be seen in The Appendix. When T_r can be ignored, starting is independent of N. Equations (4) and (6) were solved by the Adams-Moulton method –a standard numerical technique for ordinary differential equations - to obtain the solid line in Fig. 4, which accurately predicts the initial, 11 s period of slow, approximately constant acceleration. The calculations then become inaccurate because (5) is no longer valid. However, it is clear that starting is dominated by the long period of slow acceleration followed by a much shorter period of rapid acceleration during which the turbine reaches the rotor speed for power production. An important consequence of (4) and (6) which is independent of the form for blade lift and drag, comes from the scaling outside the integral: if T_s is the time required to reach a particular Ω for power extraction to commence, which is the most common strategy for small turbines, then $T_s \sim U^{-2}$. Alternatively, if power extraction starts at a fixed λ, $T_s \sim U^{-1}$. Thus the minimum starting time from Fig. 4 is approximately 40 s at the desirable cut-in wind speed of 3m/s. It is noted that this turbine is believed to be the first whose blades were designed for rapid starting

Knowing T_s as a function of U allows a simple determination of $E_g(U)$, the energy gained by motor-starting when compared to aerodynamic starting, on the basis of the following assumptions:

1. there is no resistive or cogging torque in the drive train and generator

2. motor/generator efficiency =100%

3. all grid power goes to accelerate the rotor

4. the motoring power is the turbine maximum (rated) power

5. $T_a \ll T_m$ during motoring and can be ignored, where T_m is the motoring torque

6. the turbine switches instantaneously from motoring to generating when $\lambda = \lambda_{opt}$

The energy gain is the product of the difference between the motor-starting and aerodynamic-starting times and the power output at wind speed U minus the energy required to accelerate the rotor. Thus

$$E_g(U) = P(U)[T_a(U) - T_m] - \frac{1}{2}J\Omega_s^2 \tag{7}$$

where T_m is independent of U from assumption 5. From 3 and 4:

$$P(U_r)T_m = \frac{1}{2}J\Omega_s^2 \tag{8}$$

Therefore

$$E_g(U) = P(U)T_a(U) - \frac{1}{2}J\Omega_s^2[1 + P(U)/P(U_r)] \tag{9}$$

Assume $P(U) = k_1 U^3$ as in Equation (1) with $k_1 = 5.6$ to give 5.6 kW at $U_r = 10$ m/s. Also $T_a = k_2/U$, where $k_2 = 132$ to fit the starting data. If Ω_s corresponds to λ_{opt}, then

$$\frac{1}{2}J\Omega_s^2 = \frac{J\lambda_{opt}^2 U^2}{2R^2} \tag{10}$$

and

$$E_g(U) = \left[k_1 k_2 - \frac{J\lambda_{opt}^2}{2R^2}\{1 + (U/U_r)^3\}\right]U^2 \tag{11}$$

For the 5.6 kW turbine documented in the Appendix, $J = 18$ kgm^2, $\lambda_{opt} = 7$, and $R = 2.5$ m. Thus

$$E_g(U) = 70.56[10.48 - \{1 + (U/U_r)^3\}]U^2 \tag{12}$$

It will be shown below that (12) is a good approximation for $E_g(U)$. Since $(U/U_r)^3 \leq 1$, $E_g(U)$ is positive for all values of U. It is this result that makes motor-starting attractive provided the turbine power electronics allows bi-directional power flow.
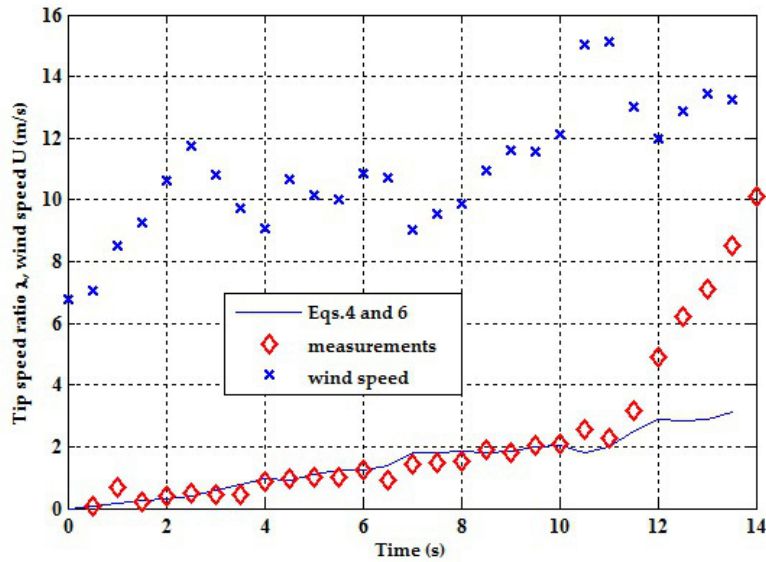
Figure 4. Measured starting sequence of a 5.0 kW two bladed wind turbine which corresponds to the starting torque of Figure 2.

4. Description of the generator and converter

4.1. Permanent magnet synchronous generator

The PMSG model is developed in the *d-q* reference frame to eliminate the time varying inductances assuming a sinusoidal distribution of the permanent magnet flux in the stator and surface mounted round rotor [18]:

$$V_q = -(R_s + pL_q)I_q - \Omega L_d I_d + \Omega \lambda_m \tag{13}$$

$$V_d = -(R_s + pL_d)I_d - \Omega L_q I_q \tag{14}$$

$$T_g = -1.5 P \lambda_m I_q \tag{15}$$

$$T_a - T_g = J d\Omega / dt \tag{16}$$

where Equation (16) is Equation (6) restated for completeness. L_d and L_q are the *d* and *q*-axis inductances, respectively; R_s is the stator winding resistance; I_d, I_q, V_d and V_q are the *d* and *q* axis currents and voltage respectively; λ_m is the amplitude of the flux induced by the permanent magnets of the rotor in the stator phases; *P* is the number of pole pairs; T_e is the electromagnetic torque. Equation (16) is a basic representation of rotor dynamics which governs the rotor acceleration, neglecting friction and other losses.

The PMSG operation mode depends on the direction of T_g: positive for generating and negative for motoring. T_g is controlled through the backward VSMC. The parameters of the 5.6 kW PMSG used in simulation are shown in the Appendix. These parameters are close to those of the 5 kW PMSG in [19] with the exception of the rated speed which has been altered to be closer to the experimental turbine which used induction generator instead of PMSG.

4.2. Very Sparse Matrix Converter

The VSMC has high efficiency, compact size, a long life span, low input current harmonics, and excellent input and output power quality control without commutation problems [20]. The VSMC provides a continuous transformation from AC-to-AC with adjustable voltage and frequency. The converter can operate in four quadrants and has the ability to shape current to be nearly sinusoidal at both the converter input and at the output using small AC filtering components. The displacement factor can be adjusted to unity by proper pulse width modulation (PWM) control [21]. The very sparse matrix converter is considered a high power density converter due to the lack of DC-link capacitors and has fewer bi-directional switches than the conventional matrix converter which also reduces the system cost [22, 23]. Moreover, the rectifier stage is commutated at zero current providing increased efficiency of the converter by reducing switching losses [24]. Note that the sophisticated control algorithms that we propose for the backward connected VSMC can be implemented at low production cost due to the advances is digital signal processor technology in recent years. At the turn of the century industry preferred the use integer digital signal processors to reduce controller cost. Today (2012), floating point digital signal processors are now quite economical and thus allow the use of sophisticated control in small wind power systems.

4.2.1. Rectifier stage of the VSMC

Many aspects must be taken into consideration in synthesizing the rectifier switching signals [13]. Figure 5 shows the modulation strategy of the rectifier PWM switching signal generation. Each grid cycle is divided to six sectors; in each sector, two of the grid side terminals are connected to either the positive or negative bus of the DC-link while the third terminal is connected to the opposite DC-link. In order to produce the maximum DC-link voltage, the maximum positive input voltage is connected to the positive bus of the DC-link for a complete 60° while the other phases are modulated to the negative DC-link bus and vice versa. So, the DC-link voltage is formed from the line to line voltage of the supply. Assuming a balanced symmetrical AC grid:

$$U_a = U_m \cos(\omega_i t)$$
$$U_b = U_m \cos(\omega_i t - 2\pi/3)$$
$$U_c = U_m \cos(\omega_i t - 4\pi/3)$$

(17)

where U_m is the maximum grid input voltage and ω_i is the grid frequency in rad/s. The DC-link voltage varies as the supply varies:

$$U_{dc} = \frac{3U_m}{2\cos(\omega_i t)} \tag{18}$$

Figure 6 shows the space vector of the grid voltage and current. If the phase angle between the space vector of the voltage and current is set to zero, unity displacement factor is achieved. The input current space vector I_i is generated by the projection to the adjacent space vectors I_α and I_β following the grid sinusoidal voltages. The duty cycles of I_α and I_β are calculated as follows:

$$d_{\alpha r} = m_i \sin(\pi/3 - \theta_i) \tag{19}$$

and

$$d_{\beta r} = m_i \sin\theta_i \tag{20}$$

where m_i is the current modulation index which is adjusted to unity to provide the maximum injected current into the grid and maximize the DC-link voltage. In order to commutate the rectifier at zero current, the inverter space vector and switching pattern should be determined and matched with the rectifier space vector to ensure that the rectifier can be switched during the period of inverter zero voltage.

4.2.2. Inverter stage of the VSMC

Switching signals of the inverter stage are generated by FOC based space vector modulation which allows use of a zero voltage vector between the transitions from negative to positive bus. It also provides a chance to distribute the vectors symmetrically to reduce the current distortion and commutate the rectifier stage at zero current to reduce the switching losses [13, 24]. The error between the actual and reference current is compensated by a proportional plus integral (PI) controller to form the generator voltage and frequency to match the operating point which is considered the reference voltage. The reference voltage is transformed to a reference space vector. The amplitude of the vector and its angle determine the active vectors which are used to form the switching signal. The amplitude of the output voltage is proportional to the input voltage according to the transfer ratio of the matrix converter:

$$U_o \leq \frac{\sqrt{3}}{2} m_c U_m \tag{21}$$

where U_o is the output maximum voltage and m_c is the VSMC conversion ratio ($0 \leq m_c \leq 1$). Fig. 7-a presents the inverter space vectors which are used to form the generator or motor voltage. Fig. 7-b shows an example of the switching signals during one sampling period assuming the reference voltage is in sector 1.
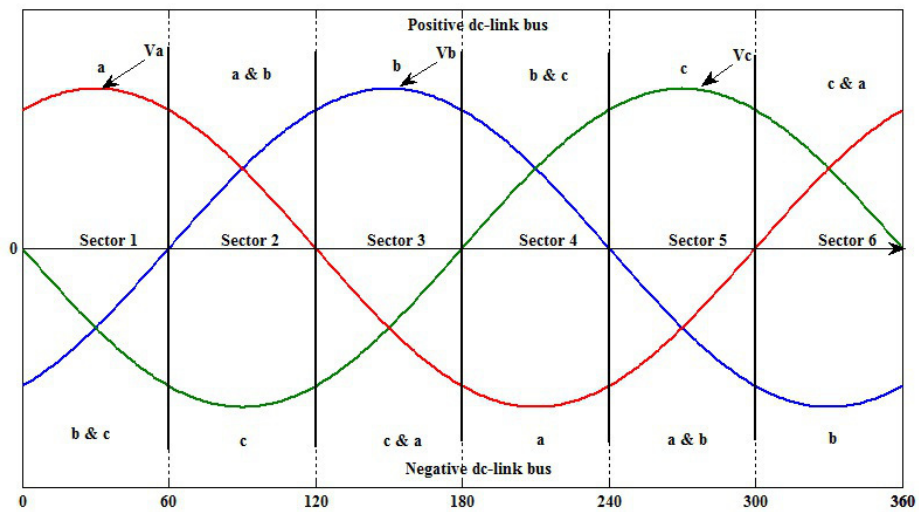
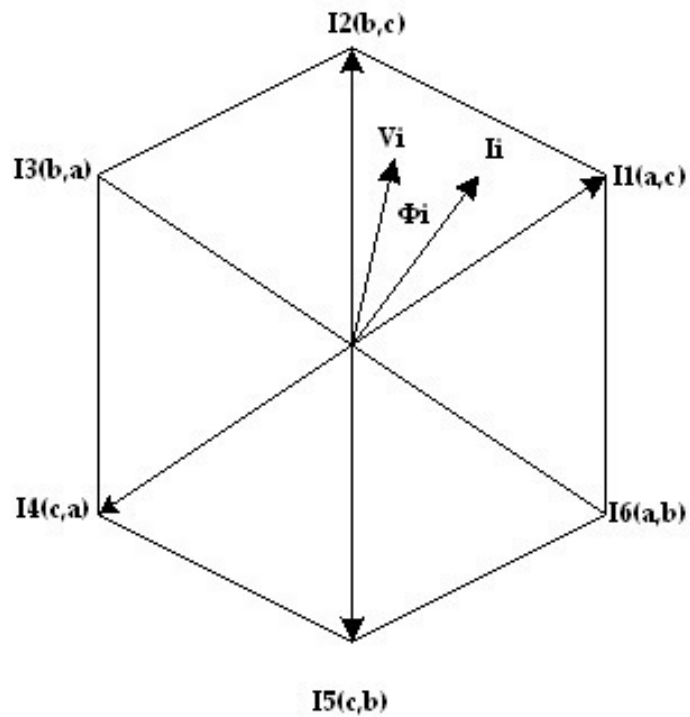**Figure 5.** Modulation strategy of the rectifier stage.

Figure 6. Rectifier stage space vector diagram

Duty cycles of the working vectors are calculated as follows depending on the space vector angle and magnitude.

$$d_{\alpha i} = m_v \sin(\pi / 3 - \theta_o) \tag{22}$$

$$d_{\beta i} = m_v \sin(\theta_o) \tag{23}$$

and

$$d_0 = 1 - d_{\alpha i} - d_{\beta i} \tag{24}$$

where $d_{\alpha i}$ and $d_{\beta i}$ represent the duty cycle of the active vectors while d_0 represents the duty cycle of the zero vector.

4.2.3. Backward VSMC

In order to guarantee the transformation of power from the generator to the grid, the DC-link voltage must be held at a fairly constant and sufficiently high average value. Given a variable wind speed and MPPT, the generator operates at variable frequency and variable voltage amplitude which is often less than the corresponding grid voltage. Due to the lack of the DC-link capacitor, the VSMC cannot operate as a boost converter to keep the DC-link voltage at the required minimum value. If employed in its forward configuration, the VSMC can be considered a step down converter according to equation (21) -. So, if the generator is connected in the conventional manner to the rectifier stage and the grid is connected to the inverter stage, (i.e. forward VSMC operation), the converter will operate only when the generator operates at its rated condition, i.e. with the wind speed at or above its rated value (to solve this problem, for a forward configuration of the VSMC, a transformer with a very large step-up ratio would be required for the grid interface) To overcome this problem (i.e. with a lower ratio step-up transformer at the grid interface) a backward connected VSMC system is proposed in [13] where the rectifier stage is connected to the grid and the inverter stage is connected to the generator as shown in Figure 1. In backward operation of the VSMC, the rectifier stage converts the grid AC voltage to a near-constant average DC voltage at the DC-link (variations in the average voltage correspond to variations in the grid voltage) while the inverter steps down the DC-link voltage to variable AC voltage with variable frequency depending on the generator and turbine operating point. In other words, the backward VSMC can be considered a step up converter from the generator side to the grid side. Such operation can be achieved by controlling the modulation index of the inverter stage to boost the generator voltage to the grid voltage depending on the operating speed. This configuration has the merits that control of the DC voltage is not needed, nor is synchronization with the grid required. Voltage flicker is not an issue due to the small filter on the mains side of the converter. The generator voltage and the grid current are synthesized using a space vector PWM technique with the guarantee of injecting current into the grid with or without reactive power to meet the grid power quality requirements as explained in next subsections.
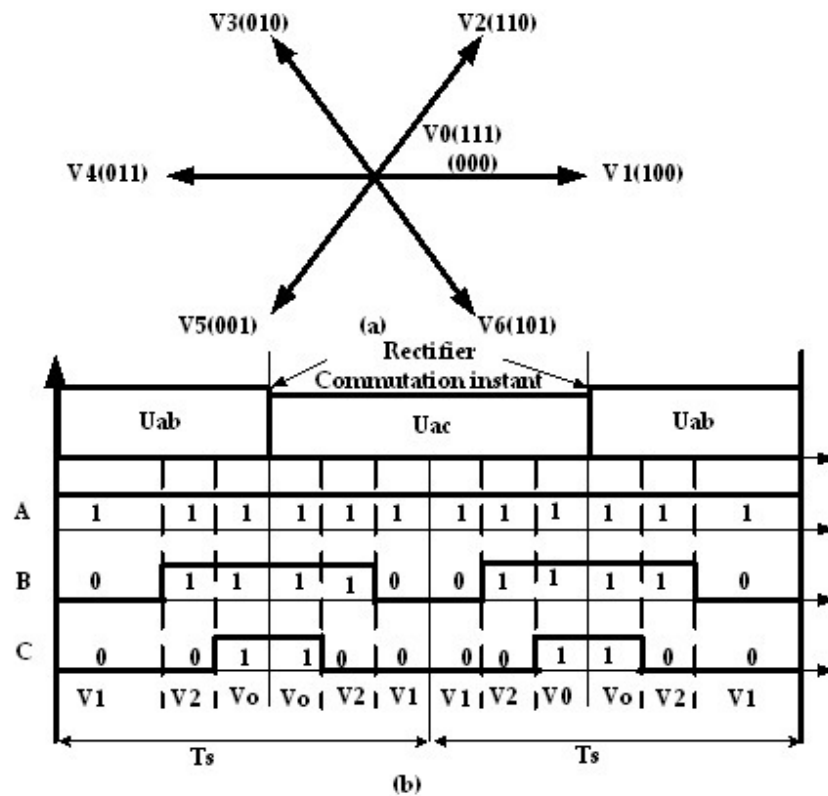
Figure 7. a) Inverter space vector diagram (b) Inverter switching signal for sector 1.

4.3. Motoring-generating mode

Equation (15) shows that the torque direction and hence the generator mode can only be controlled by the quadrature current component direction. In addition the torque is also controlled by the magnitude of I_q to match the wind power at different wind speeds. The amplitude and the direction of the generator quadrature current I_q can be controlled through the inverter stage of the VSMC.

The VSMC can operate the generator as a motor using FOC by controlling the current component which corresponds to the torque limited only by the generator torque rating. Figure 8 shows the flow chart of the starting strategy. The controller produces the reference generator current depending on the mode of operation, either motor starting or generator mode (MPPT control). If in motor starting mode, the actual and reference motor currents are compared to generate the proper machine voltage vector which results in rated torque operation of the machine. Once the turbine reaches the nominated speed, Ω_{ref}, corresponding to λ_{opt}, motoring ceases and generating with MPPT control is enabled. Figure9 shows the proposed control technique for motor starting.
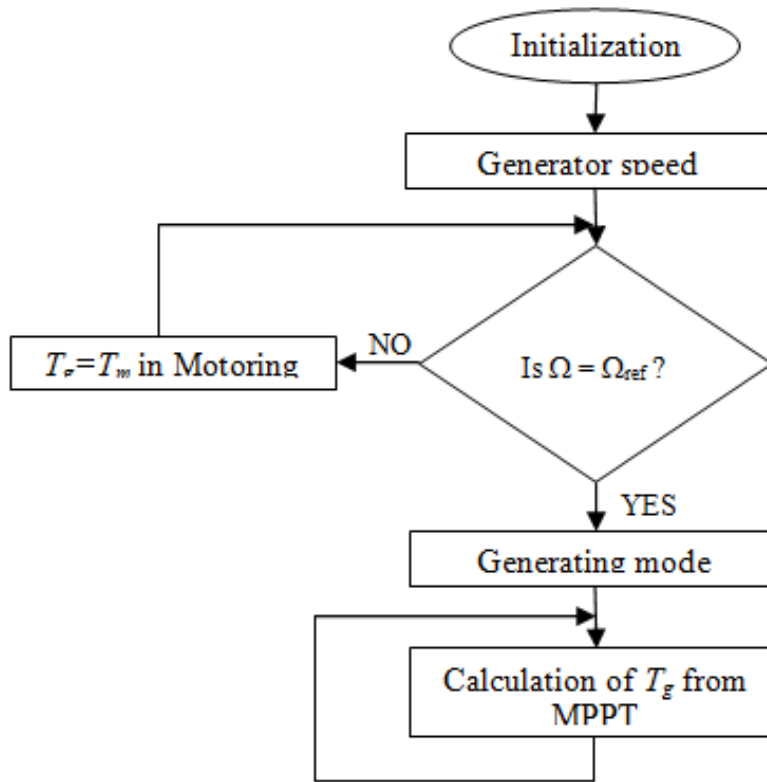
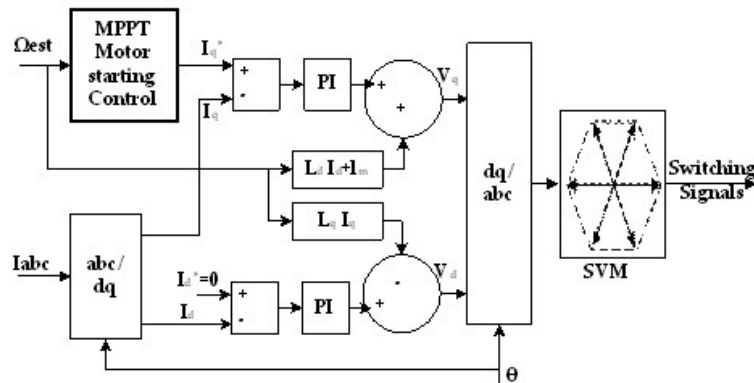**Figure 8.** Starting strategy flow chart.

Figure 9. Block diagram of the generator-motor FOC technique.

5. Simulation results and discussion

The system described above was simulated using MATLAB Simulink for the 5.6 kW turbine described in the Appendix, initially for a wind speed is 10 m/s. Figure 10 shows results for

aerodynamic starting where the generator torque is zero up to the λ_{opt}. Then the generator torque closely matches the aerodynamic torque and power production starts. In Figure 11, the turbine is motored to λ_{opt}. The significant reduction in starting time is obvious.

As shown in Figure 11 10, the current is held positive and constant at its rated value during motoring. It is then changed to a negative value corresponding to the wind speed to run as a generator while for aerodynamic starting the current is kept zero then increased in negative direction to the value which matches with the aerodynamic torque. As shown in Figure 10 and 11, the rotor takes 13.29 s to reach λ_{opt} when starting aerodynamically, which is consistent with the field test data in Fig. 4, while it takes 1.9 s for a motored start. The significant difference results in a significant gain in energy harvested.

In both starting cases, the turbine runs at the maximum C_p of 0.476 after λ reaches λ_{opt}. The MPPT would re-establish this C_p if U subsequently changes. Whether in motoring or generating mode, the grid current is sinusoidal due to the operating characteristics of the VSMC and its phase angle can be controlled depends on the direction of power flow and if desired unity power factor can be achieved to insure the power quality.
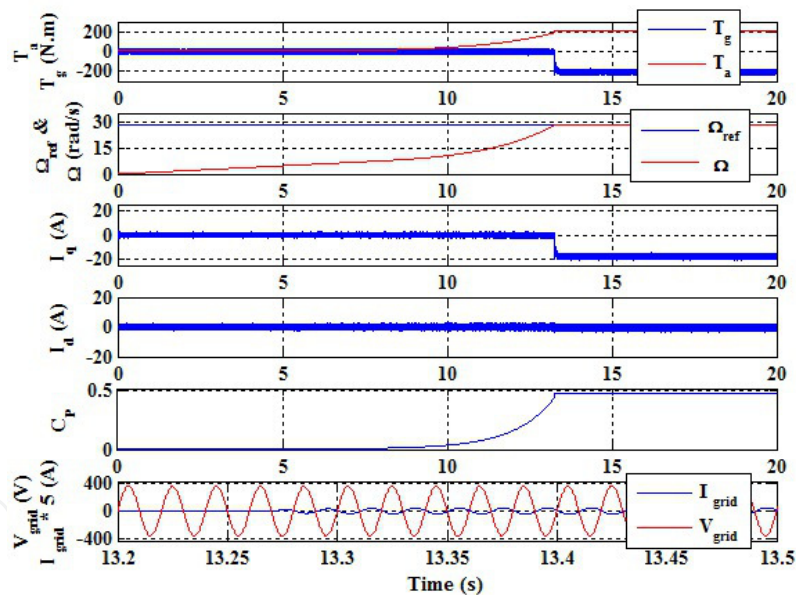

Figure 10. Aerodynamic starting of the 5.6 kW wind turbine for a wind speed of 10 m/s.

As shown in Fig. 12, for all wind speeds, motor starting reduces the starting time. Fig. 12 also shows the starting time when power production commences at a fixed fraction of the rotor maximum speed which is common operational practice for small wind turbines. Fig. 13 indicates that there is a net gain in energy delivered to the grid for motor starting compared to aerodynamic starting. As seen in Fig. 13, provided the turbine is rotating sufficiently fast, the shaft speed at which the controller switches from motor mode to generator mode does not significantly alter the energy gain compared to aerodynamic starting. This is valua-

ble for the practical implementation of the proposed approach since the wind speed does not need to be measured to determine the length of duration of the motoring mode. Motor starting can also reduce the starting wind speed, allowing the turbine to start and then produce power down to 1 m/s.
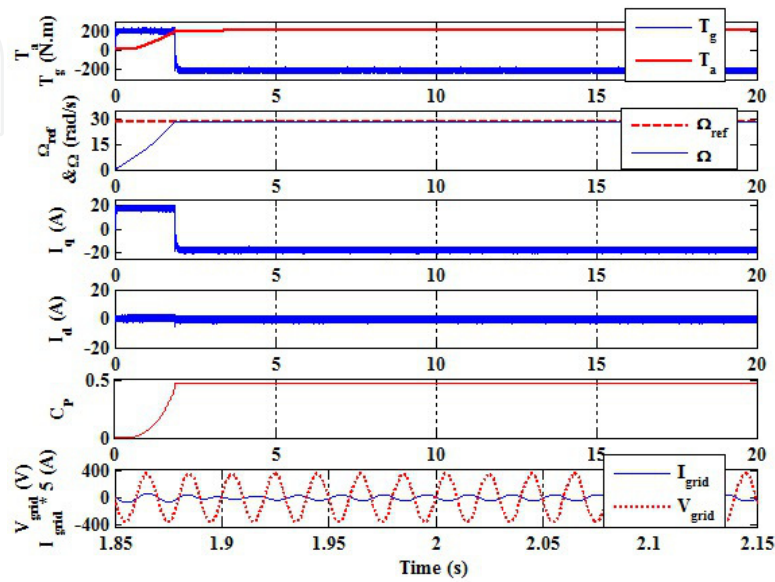

Figure 11. Motor starting of the 5.6 kW wind turbine for a wind speed of 10 m/s.
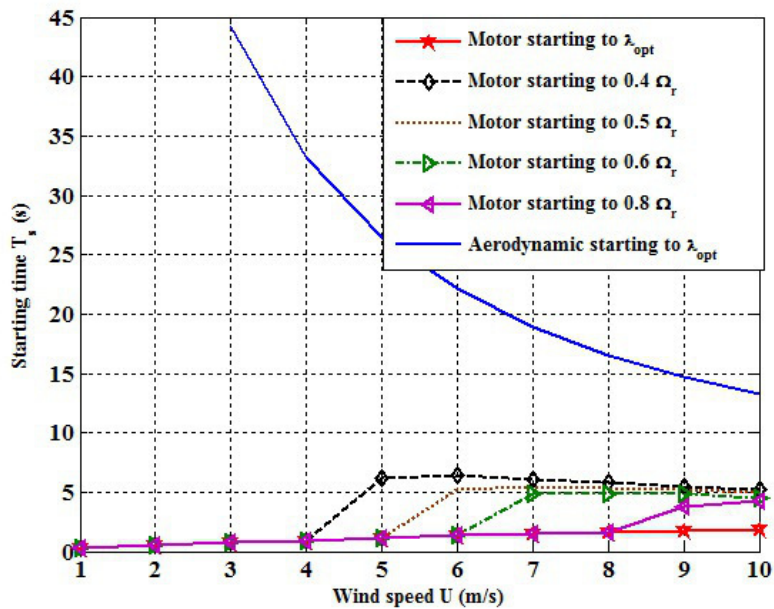

Figure 12. Starting time for aerodynamic and motor starting.

At this point, it is too early to determine the cost effectiveness of the motor starting approach partly because we have not yet done any simulations to test its effectiveness in realistic low-wind conditions. It is also difficult to ascertain the net energy gain over a substantial time (e.g. one year of operation). Nonetheless, as power electronics continue to quickly drop in cost [5], the use of a wind turbine in a variable speed mode of operation with an accompanying power converter seems increasingly attractive, and techniques such as motor starting may be a part of the role that power electronics can serve.
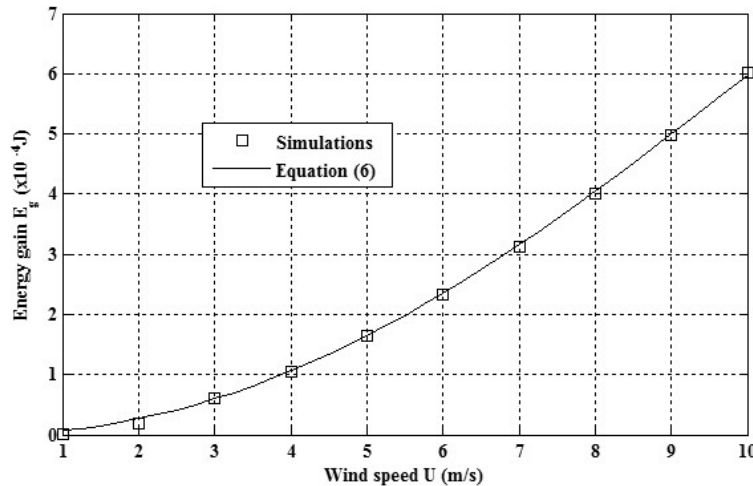

Figure 13. Energy gain by motor-starting to $\lambda_{opt.}$

6. Summary and future developments

Power electronics are developing rapidly and their cost is falling. These trends will continue to be used to reduce the cost of small wind turbines and improve their cost effectiveness. After briefly noting these trends, this Chapter concentrated on a modern converter topology suitable for grid connected small wind turbines: the backward very sparse matrix converter (VSMC). It has the potential to improve conversion efficiency by reducing switching losses. In turn, the ability to switch rapidly in a complex fashion has been made possible by recent improvements in digital signal processing technology. Like many modern topologies, the VSMC allows bi-directional power flow which can be exploited to motor start a small wind turbine and increase the energy extracted, at least for the artificial case of a step increase in the wind speed from zero. The strategy also lowers the cut-in wind speed and shows the importance of considering the whole turbine system when designing the converter.

Motor starting as the wind speed increased was analyzed to compare with conventional aerodynamic starting assessed experimentally for a 5.0 kW wind turbine whose blades were designed to start quickly. Using the scaling outside the integral in Equation (5), the aerodynamic starting at any wind speed was determined. The simple analysis of Section 4 and the

detailed Simulink modeling both show that an energy gain occurs for all wind speeds with motor starting. Moreover, the turbine can contribute energy to the grid at wind speeds below the conventional cut-in speed if motoring is employed. This strongly suggests that motor-starting should be investigated for more typical wind speed variations. The results suggest a good practical strategy is to motor the turbine to 60% of rated rotor speed when the average wind speed is in the range of 4 to 7 m/s [26].

Acknowledgements

Appendices

Appendix – Parameter Values used in Simulations

Grid Parameters	
Phase Voltage (rms)	220 (V)
Frequency	60 (Hz)
5.6 kW PMSG Parameters [12]	
Rated phase voltage (rms)	165 (V)
Phase current (rms)	12 (A)
Rated frequency	36 (Hz)
Rated torque	204.2 (Nm)
Rated speed	270 (rpm)
L_d, L_q	0.02047(mH)
R_s	1.5 (ohm)
Magnet flux	0.97 (wb)
pole pairs	8
inertia	0.138 (Kgm^2)
5.6 kW Wind Turbine Parameters [10]	
Rotor diameter, R	5 (m)

Rotor rated speed, Ω_r			270 (rpm)
Cut-in wind speed			2.5 (m/s)
Rated wind speed			10 (m/s)
Inertia, J			18(Kgm^2)
Maximum C_p			0.475
λ_{opt}			7
$a_0 = 0.0061$	$a_1 = -0.0013$	$a_2 = 0.0081$	$a_3 = -9.75 \times 10^{-4}$
$a_4 = -6.54 \times 10^{-5}$	$a_5 = 1.30 \times 10^{-5}$	$a_6 = -4.54 \times 10^{-7}$	

Author details

Mohamed Aner[1], Edwin Nowicki[1] and David Wood[2*]

*Address all correspondence to: dhwood@ucalgary.ca

1 Dept Electrical and Computer Engineering, Canada

2 Dept Mechanical and Manufacturing Engineering, University of Calgary, Calgary, T2N 1N4, Canada

References

[1] Small Wind Systems UK Market Report. (2011, April). *British Wind Energy Association*, available:, http://www.bwea.com/pdf/small/Small_Wind_Systems_Market _Report_2011.pdf.

[2] Tirumara, R., & Mohan, N. (2000, April 3-7). Dynamic simulation and comparison of slip ring induction generators used for wind energy generation. Paper presented at International Power Electronics Conference, Tokyo. 956-965.

[3] Carlin, P. W., Laxson, A. S., & Muljadi, E. B. (2001, Feb). The history and state of the art of variable-speed wind turbine technology. *National Renewable Energy Laboratory*, 10.2172/776935.

[4] Zaragozaa, J., Poua, J., Ariasa, A., Spiterib, C., Roblesc, E., & Ceballos, S. (2011, May). Study and experimental verification of control tuning strategies in a variable speed wind energy conversion system. *Renewable Energy*, 36(5), 1421-1430.

[5] Ivov, F., & Blaabjerg, F. (2009). Power electronics and control for wind power systems. IEEE Power Electronics and Machines in Wind Applications (PEMWA09) Lincoln, Nebraska, June 24-26 , 1-16.

[6] Ebert, P. R., & Wood, D. H. (1997, Nov). Observation of the start-up behavior of a small horizontal-axis wind turbine. *Renewable Energy*, 12, 245-257.

[7] Mayer, C., Bechly, M. E., Hampsey, M., & Wood, D. H. (2001). The start-up behaviour of a small horizontal-axis wind turbine. Renewable Energy March, 22, 411-417.

[8] Kjellin, J., & Bernhoff, H. (2011). Electrical starter system for an h-rotor type VAWT with PM-generator and auxiliary winding. Journal of Wind Engineering Feb., 35, 85-92.

[9] Hill, N., Dominy, R., Ingram, G., & Dominy, J. (2009). Darrieus turbines: the physics of self-starting. *Proc. IMechE Part A: Journal of Power and Energy*, 223, 21-29.

[10] Wood, D. H. (2011). Small Wind Turbines: Analysis, Design, and Application,. Springer-Verlag, London, 10.1007/978-1-84996-175-2.

[11] Wright, A. K., & Wood, D. H. (2004, Dec). The starting and low wind speed behavior of a small horizontal axis wind turbine. *Journal of Wind Engineering and Industrial Aerodynamics*, 92, 1265-1279.

[12] Qin, S., Wang, M., Chen, T., & Yao, X. (2011, Sept 16-18). Comparative analysis of incremental conductance and perturb-and observation methods to implement MPPT in photovoltaic system. Paper presented at Proc. 2011 International Conference on Electrical and Control Engineering (ICECE),. 5792-5795.

[13] Aner, M., & Nowicki, E. (2011). Two-level backward operation of VSMC for PMSG grid connected variable speed wind turbine systems. in Proc. 2011 IEEE International Electric Machines and Drives Conf., (IEMDC11) Niagara Falls, Canada , 1116-1122.

[14] Motto, E. R., Donlon, J. F., Tabata, M., Takahashi, H., Yu, Y., & Majumdar, G. (2004). Application characteristics of an experimental RB-IGBT (reverse blocking IGBT) module. Paper presented at IEEE Industry Applications Society Annual Meeting, Seattle. 3, 1540-1544.

[15] Takei, M., Odaka, A., & Fujimoto, H. ((2002). Application technologies of reverse-blocking IGBT. Fuji Electric Journal , 75(8)

[16] Itoh, J., Odaka, A., & Sato, I. (2004). High efficiency power conversion using a matrix converter. *Fuji Electric Review*, 50(3), 94-98.

[17] Munteanu, I., Bratcu, A. L., Cutululis, N. A., & Ceanga, E. (2008). Optimal Control of Wind Energy Systems. 1st Ed.Springer-Verlag London , 243.

[18] Tan, K., & Islam, S. (2004). Optimum control strategies in energy conversion of PMSG wind turbine system without mechanical sensors. IEEE Transactions on Energy Conversion June, 19(2), 392-400.

[19] Wu, B., Lang, Y., Zargaria, N., & Kouro, S. (2011). Power Conversion and Control of Wind Energy Systems. Wiley IEEE press, 10.1002/9781118029008.

[20] Itoh, J., Odaka, A., & Sato, I. (2004). High efficiency power conversion using a matrix converter. *Fuji Electric Review*, 5(3), 94-98.

[21] Wheeler, P. W., Rodriguez, J., Clare, J. C., Empringham, L., & Einstein, A. (2002). Matrix converters: a technology review. IEEE Trans. Industrial Electronics April., 49, 276-288.

[22] Kolar, J., Baumann, M., Schafmeister, F., & Ertl, H. (2002). Novel three-phase ac-dc-ac sparse matrix converters- Part I and II. Paper presented at IEEE Applied Power Electronics Conference, Dallas. 777-791.

[23] Kolar, J. W., Schafmeister, F., Round, S. D., & Ertl, H. (2007, Sept). Novel three-phase ac/ac sparse matrix converters,. *IEEE Trans. Power Electronics*, 22, 1649-1661.

[24] Wei, L., & Lipo, T. A. (2001). A novel matrix converter topology with simple commutation,. IEEE Industry Applications Society Annual Meeting Chicago , 1749-1754.

[25] Cha, H. J., & Enjeti, P. N. (2004, July-Aug). Matrix converter-fed ASDs. *IEEE Industry Applications Magazine*, 10, 33-39.

[26] Aner, M., Nowicki, E., Ali, A., & Wood, D. H. (2012). Sensor-less Motor Starting of Grid-Connected Small Wind Turbine. in Proc. RAEPS, April, Alexandria, Egypt.